AGU PUBLICATIONS

Geophysical Research Letters

RESEARCH LETTER
10.1002/2016GL069836

Key Points:
- Spin and valence states of Fe in bridgmanite are investigated by X-ray emission and Mössbauer up to 115 GPa after laser annealing
- Fe^{2+} and Fe^{3+} are in the high-spin state in the A site of bridgmanite lattice and remain stable throughout the lower mantle
- (Fe,Al)-bearing bridgmanite will not exhibit elastic anomalies associated with the spin transition, in contrast to ferropericlase

Supporting Information:
- Supporting Information S1

Correspondence to:
J.-F. Lin and Z. Mao,
afu@jsg.utexas.edu;
zhumao@ustc.edu.cn

Citation:
Lin, J.-F., Z. Mao, J. Yang, J. Liu, Y. Xiao, P. Chow, and T. Okuchi (2016), High-spin Fe^{2+} and Fe^{3+} in single-crystal aluminous bridgmanite in the lower mantle, *Geophys. Res. Lett.*, *43*, 6952–6959, doi:10.1002/2016GL069836.

Received 31 MAY 2016
Accepted 28 JUN 2016
Accepted article online 1 JUL 2016
Published online 14 JUL 2016

High-spin Fe^{2+} and Fe^{3+} in single-crystal aluminous bridgmanite in the lower mantle

Jung-Fu Lin[1,2], Zhu Mao[3,4], Jing Yang[1], Jin Liu[1], Yuming Xiao[5], Paul Chow[5], and Takuo Okuchi[6]

[1]Department of Geological Sciences, Jackson School of Geosciences, University of Texas at Austin, Austin, Texas, USA, [2]Center for High Pressure Science and Technology Advanced Research (HPSTAR), Shanghai, China, [3]Laboratory of Seismology and Physics of Earth's Interior, School of Earth and Planetary Sciences, University of Science and Technology of China, Hefei, China, [4]National Geophysics Observatory, Mengcheng, China, [5]HPCAT, Geophysical Laboratory, Carnegie Institution of Washington, Argonne, Illinois, USA, [6]Institute for Planetary Materials, Okayama University, Misasa, Japan

Abstract Spin and valence states of iron in single-crystal bridgmanite ($Mg_{0.89}Fe_{0.12}Al_{0.11}Si_{0.89}O_3$) are investigated using X-ray emission and Mössbauer spectroscopies with laser annealing up to 115 GPa. The results show that Fe predominantly substitutes for Mg^{2+} in the pseudo-dodecahedral A site, in which 80% of the iron is Fe^{3+} that enters the lattice via the charge-coupled substitution with Al^{3+} in the octahedral B site. The total spin momentum and hyperfine parameters indicate that these ions remain in the high-spin state with Fe^{2+} having extremely high quadrupole splitting due to lattice distortion. (Al,Fe)-bearing bridgmanite is expected to contain mostly high-spin, A-site Fe^{3+}, together with a smaller amount of A-site Fe^{2+}, that remains stable throughout the region. Even though the spin transition of B-site Fe^{3+} in bridgmanite was reported to cause changes in its elasticity at high pressures, (Fe,Al)-bearing bridgmanite with predominantly A-site Fe will not exhibit elastic anomalies associated with the spin transition.

1. Introduction

Electronic transitions of iron in lower mantle minerals have attracted significant interest in application to understanding the geophysics, geochemistry, and geodynamics of the deep lower mantle [e.g., *Badro et al.*, 2003; *Lin et al.*, 2005; *Speziale et al.*, 2005; *Cammarano et al.*, 2010; *Yang et al.*, 2015], but the nature of the spin transitions of iron in bridgmanite remains in question experimentally [*Lin et al.*, 2013]. The spin transition of iron in ferropericlase has been indisputably established in first-principle theoretical calculations and by observations in high-pressure diamond anvil cell (DAC) experiments, including the collapse of the Fe Kβ satellite peak in X-ray emission spectroscopy (XES), the disappearance of the quadrupole splitting (QS) in Mössbauer spectroscopy (MS), and the volume decrease in X-ray diffraction (XRD) [e.g., *Badro et al.*, 2003; *Lin et al.*, 2005; *Speziale et al.*, 2005; *Mao et al.*, 2011; *Lin et al.*, 2013; *Yang et al.*, 2015]. In contrast, the spin and valence states of iron in the lower mantle bridgmanite, the most abundant mineral in the planet, have also been extensively investigated using the same approaches, but literature experimental results cannot be simply reconciled with theoretical predictions and have remained controversial (see *Lin et al.* [2013] for a recent review).

The major challenge in deciphering the valence and spin states of iron in bridgmanite can be traced to its rather complex crystal chemistry, in which iron ions can occupy two crystallographic sites [e.g., *Vanpeteghem et al.*, 2006; *Lin et al.*, 2013]. Magnesium bridgmanite ($MgSiO_3$) has a distorted orthorhombic crystal structure, in which Mg^{2+} occupies the large pseudo-dodecahedral (8/12-fold) A site and Si^{4+} resides in the smaller 6-fold, octahedral B site. Previous experimental and theoretical results have shown that Fe^{2+} mainly substitutes for Mg^{2+} in the A site, whereas Fe^{3+} can occupy both A and B sites, in which the abundance and site occupancy of Fe^{3+} depends on the amount of Al-Si substitution [e.g., *McCammon*, 2006; *Vanpeteghem et al.*, 2006; *Hsu et al.*, 2010, 2011, 2012; *Hsu and Wentzcovitch*, 2014; *Mohna and Trønnesa*, 2016]. In the pyrolite lower mantle, bridgmanite can contain 5–10 mol% Al^{3+} in the B site; such that, most Fe^{3+} are energetically favorable to occupy the A site via the charge-coupled substitution, $Mg^{2+} + Si^{4+} = Fe^{3+} + Al^{3+}$ [e.g., *Hummer and Fei*, 2012; *Potapkin et al.*, 2013]. High-pressure studies have observed the occurrence of the extremely high QS values of Fe^{2+} in the A site (as high as ~4.4 mm/s) and the partial decrease of the Fe Kβ satellite peak, which have been interpreted as evidence for an electronic spin transition or transitions in bridgmanite in the lower mantle [e.g., *Badro et al.*, 2004; *Li et al.*, 2004, 2006; *Jackson et al.*, 2005; *Bengtson et al.*, 2008, 2009; *Lin*

et al., 2008; *Grocholski et al.*, 2009; *McCammon et al.*, 2008, 2010; *Catalli et al.*, 2010, 2011; *Hsu et al.*, 2010, 2011; *Fujino et al.*, 2012, 2014]. Together with the derived total spin momentum of approximately one ($S = 1$) from XES results, the A-site Fe^{2+} has been suggested to undergo a high-spin to intermediate-spin transition at high pressures [e.g., *Lin et al.*, 2008; *McCammon et al.*, 2008, 2010]. However, it has been shown in recent first-principle calculations that the extremely high QS is a result of the pressure-induced local lattice distortion [*Bengtson et al.*, 2008, 2009; *Hsu et al.*, 2010, 2011, 2012; *Hsu and Wentzcovitch*, 2014]. Furthermore, the decrease in the Fe Kβ satellite intensity could be due to the peak broadening artifact that can contribute to an overestimation of the reduction of the total spin momentum in the XES spectral analysis [e.g., *Mao et al.*, 2014]. Based on these results, Fe^{2+} in the distorted A site preserves its high-spin electronic configuration in the lower mantle, instead of assuming the intermediate-spin state or the low-spin configuration suggested in some experimental studies. It has also been argued that Fe^{3+} in the A site with much lower QS should also remain in the high-spin state especially in Al-bearing bridgmanite, in which Fe^{3+} is expected to be predominantly in the A site [e.g., *Vanpeteghem et al.*, 2006; *Hsu and Wentzcovitch*, 2014]. Thus far, the only consensus on the spin transition of iron in bridgmanite is about the B-site Fe^{3+}, which based on combined synchrotron Mössbauer spectrum (SMS) and XES results and theoretical calculations, undergoes a high-spin to low-spin transition at high pressures, although the transition pressure in previous studies varies significantly [e.g., *Jackson et al.*, 2005; *Catalli et al.*, 2010; *Hsu et al.*, 2011; *Lin et al.*, 2012; *Mao et al.*, 2015].

These recent experimental studies have mostly relied on XES or Mössbauer spectroscopic results to investigate polycrystalline bridgmanite samples that were synthesized in a laser-heated diamond anvil cell (DAC) or in a multianvil apparatus, leading to inconsistent interpretations of the spin and valence states of iron in bridgmanite at high pressures [e.g., *Lin et al.*, 2013]. The complexity of bridgmanite's crystal chemistry where Fe adopts different valence states in different crystallographic sites as well as the sensitivity of the experimental results to nonhydrostatic environments, and spectral analysis have further hampered our understanding of the spin and valence states of iron in the lower mantle. To provide new insight on this critical topic, we have performed complementary high-pressure XES, SMS, and XRD experiments with a well-characterized single-crystal bridgmanite starting sample ($Mg_{0.89}Fe_{0.12}Al_{0.11}Si_{0.89}O_3$) with laser annealing in a DAC up to 115 GPa. Analysis of the XES spectra shows that the A-site Fe^{2+} and Fe^{3+} maintain a total spin momentum and hyperfine parameters that are characteristic of the high-spin state. A significant reduction of the Fe Kβ satellite peak was only observed from the sample under nonhydrostatic condition without laser annealing or when the peak broadening effect was not taken into account. Our results are applied to understand the role of the iron valence and spin states in bridgmanite on the geophysics and geochemistry of the deep lower mantle.

2. Experiments

Bridgmanite single crystals (run no. 5k2179) were synthesized from a mixture of starting materials including ground $MgSiO_3$, $Mg(OH)_2$, Al_2O_3, and ^{57}FeO powder in an appropriate wt % proportion of 71:17:7:5. The mixture was packed into a Pt capsule measuring 1 mm in diameter and 2 mm in length and then compressed using the 5000 t Kawai Apparatus at Institute for Planetary Materials, Okayama University, at Misasa, Japan [*Okuchi et al.*, 2015]. Starting ^{57}Fe-enriched FeO oxide with >95% enrichment was purchased from Cambridge Isotopes Inc., and used in the synthesis to permit MS measurements that complement the XES study. The sample assemblage was compressed to 24 GPa and then heated to 1750°C for 7 h to permit sufficient growth of the crystals before being quenched to ambient temperature by cutting off the power to a $LaCrO_3$ heater. After opening the Pt capsule, pale brown subhedral single crystals of bridgmanite measuring tens to approximately hundreds of micrometers in size were identified using an optical microscope. Electron microprobe and high-resolution transmission electron microprobe analyses of the crystals showed homogenous chemical distribution and well crystalline atomic arrangements without observable signs of inclusions. Analysis of the X-ray diffraction results of the sample showed the crystal having the orthorhombic unit cell parameters (space group: *Pbnm*) of $a = 4.7867(2)$ Å, $b = 4.9569(2)$ Å, and $c = 6.9141(4)$ Å at ambient conditions (Figure 1). Wavelength-dispersive electron microprobe analyses of a few representative crystals showed homogeneous chemistry with an average chemical formula of $Mg_{0.89}Fe_{0.12}Al_{0.11}Si_{0.89}O_3$. Conventional MS analysis of the crystals at ambient conditions was performed to determine the spin and valence states of Fe at ambient conditions (Figure S1 in the supporting information).

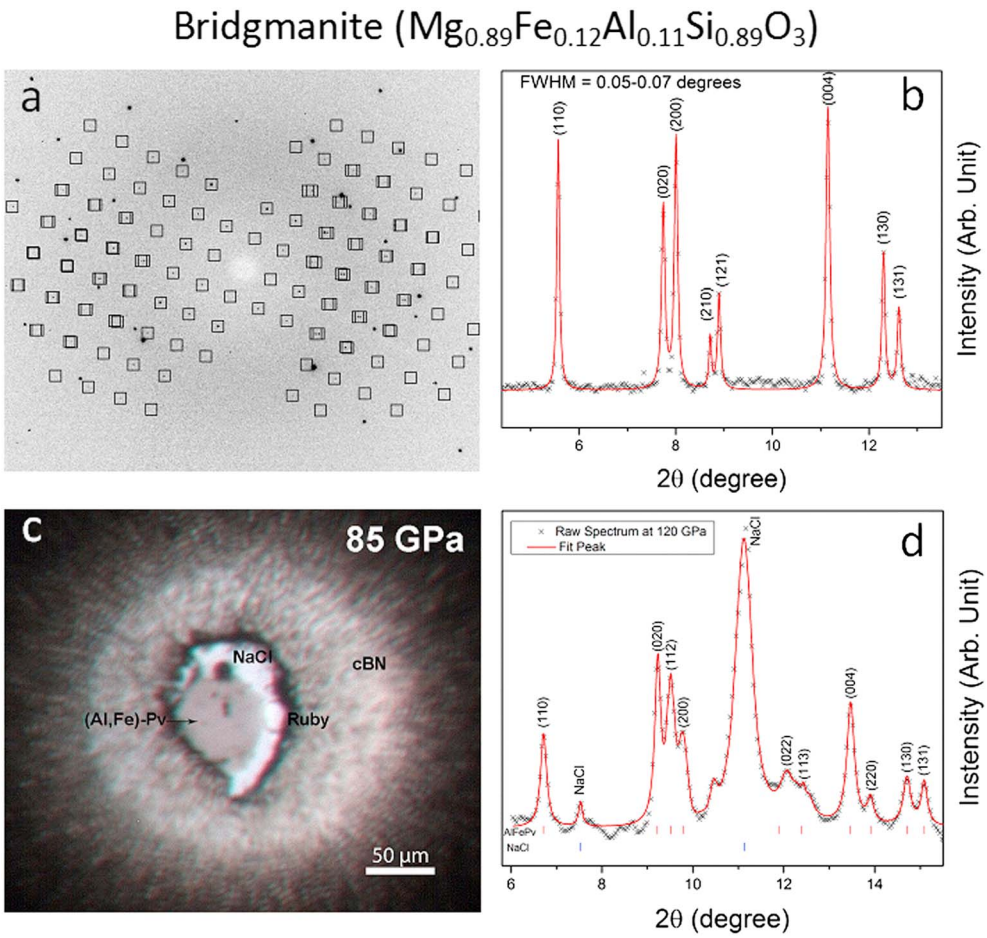

Figure 1. Representative X-ray diffraction patterns and photograph of bridgmanite ($Mg_{0.89}Fe_{0.12}Al_{0.11}Si_{0.89}O_3$). (a and b) Raw diffraction image and integrated X-ray diffraction pattern at ambient conditions, respectively. (c) A single-crystal sample loaded into a DAC at 85 GPa after laser annealing at ~1800 K for approximately 10 min and then quenched to ambient temperature. (d) X-ray diffraction pattern of the sample at 115 GPa and ambient temperature after laser annealing. X-ray wavelength was 0.3344 Å. Squares in Figure 1a are used to highlight the single-crystal diffraction spots found for the sample. All other diffraction spots without the squares in the pattern came from the diamond anvils of the DAC. Lines in Figures 1b and 1d represent the LeBail fit to the diffraction pattern shown as *x*. Miller indices of the crystal are labeled on top of their corresponding diffraction peaks.

These crystals with ~100 μm in diameter were polished from both sides of the platelet down to approximately 25 μm thick using 3 M diamond film with water as the lubricant; the use of water was intended to prevent any potential amorphization of the crystals during polishing. This surface-polishing process was considered necessary as some of the crystal surfaces may contain Fe-bearing materials as a result of high-temperature quenching that could affect MS and XES studies. The quality and orientation of the polished crystals were further examined using synchrotron XRD at the 13IDD beamline of the GeoSoilEnviroConsortium for Advanced Radiation Sources (GSECARS) of the Advanced Photon Source (APS), Argonne National Laboratory. Analysis of the diffraction images showed that the sample platelet was typically in (001) orientation with the full width at half maximum (FWHM) for each peak ranging from ~0.05 to 0.07° (Figures 1a and 1b).

Polished sample platelets were loaded into DACs with culet sizes of either 300 μm or 150–300 μm. A Be gasket of 3 mm in diameter was preindented to approximately 25 μm in thickness and drilled with a hole size of 250 μm. cBN gasket insert was then packed into the drilled hole, compressed to 25 GPa, and drilled with a hole of 80 μm in diameter which was used as the sample chamber (Figure 1c) [*Lin et al.*, 2008]. Two sets of XES experiments were performed: (1) compression of the sample in a mineral oil pressure medium at ambient temperature without laser annealing and (2) laser annealing of the crystal to ~1800 K at each given pressure,

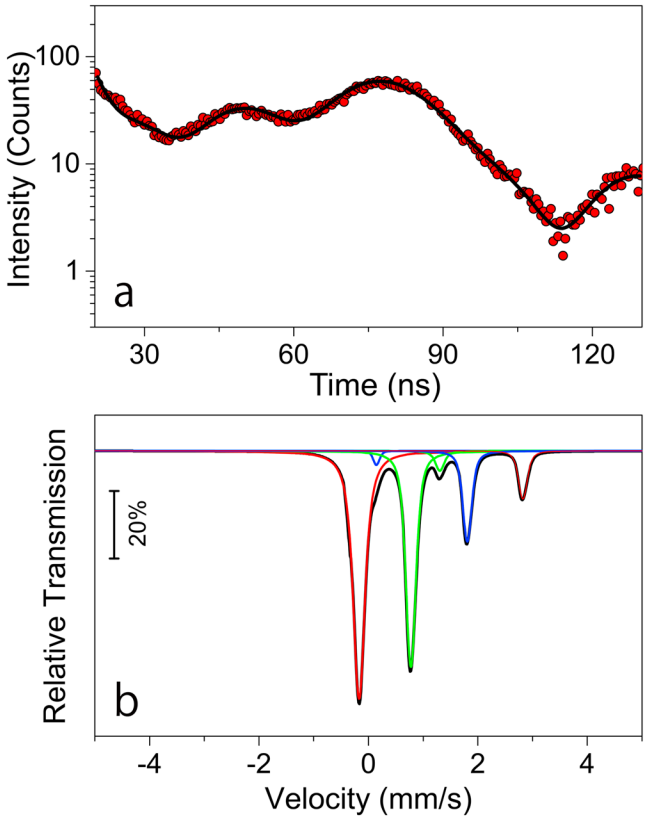

Figure 2. Representative SMS (a) and modeled energy spectrum (b) of bridgmanite ($Mg_{0.89}Fe_{0.12}Al_{0.11}Si_{0.89}O_3$) at 115 GPa and 300 K after laser annealing. The spectrum was fitted with a three-doublet model shown in relative transmission as a function of velocity.

where XES spectra were measured. In the laser-annealing experiments, the bridgmanite crystal was sandwiched between two dried NaCl layers a few micrometers thick that was also used as a pressure calibrant (Figure 1d) [*Fei et al.*, 2007]. The sample assemblage before compression was dried in a vacuum for 30 min using the gas loading system at the Mineral Physics Laboratory of the University of Texas at Austin. Laser-annealing experiments were performed at each given pressure for about 10 min prior to XES measurements using an off-line laser heating system at the GSECARS sector, while the synchrotron XRD patterns were collected using a CCD at the 13IDD beamline with an X-ray wavelength of 0.3344 Å.

High-pressure XES experiments were conducted at 16IDD sector of the High Pressure Collaborative Access Team (HPCAT) of the APS to examine the total spin momentum of Fe ions in the crystals. An incident X-ray beam with an energy of 11.35 keV, a bandwidth of ~1 eV, and a beamsize of 25 μm in diameter (FWHM) was used for the experiments. The incident X-ray was focused onto the sample through one of the diamond anvils, and the Fe Kβ emission spectra were collected by a silicon detector through the Be gasket and a Si analyzer in the 1 m Rowland circle geometry with a step size equivalent to about 0.3 eV. The collection time for each XES spectrum was about 40 min, and 5–10 spectra were collected and added together at each given pressure until the maximum intensity at the Fe Kβ main peak was more than 10,000 counts. The pressure was determined by the ruby R_1 fluorescence shifts of ruby spheres or XRD patterns of NaCl loaded in the sample chambers [*Mao et al.*, 1986; *Fei et al.*, 2007]. For laser-annealing experiments, XRD patterns of NaCl were also measured and used to determine pressures of the samples after laser annealing. Reference XES spectra for high-spin iron were collected from ferropericlase ($(Mg_{0.75}Fe_{0.25})O$) and enstatite ($(Mg_{0.9}Fe_{0.1})SiO_3$) as well as hematite (Fe_2O_3) at ambient conditions, while ferropericlase at 95 GPa and 300 K and FeS_2 were measured for the low-spin reference [*Mao et al.*, 2014].

High-pressure SMS were collected by an avalanche photodiode detector at X-Ray Operations and Research sector 3 of the APS. An incident X-ray beam with an energy of 14.4125 keV and a bandwidth of 1 meV was used to excite the ^{57}Fe nuclei in the sample (Figure 2). The SMS spectra were evaluated with the CONUSS programs to derive the hyperfine parameters, quadrupole splitting (QS), and chemical shift (CS) [*Sturhahn*, 2000].

3. Results and Discussion

XRD results of the crystals in the DAC confirmed that the samples after annealing remained in the orthorhombic structure (*Pbnm*) at the pressure range of the experiments, but the FWHM of the XRD peaks became significantly broader at high pressures even after laser annealing (Figure 1d). The Mössbauer spectrum at ambient conditions can be well represented by the two-doublet model: doublet 1 with QS = 0.91 (±0.03) mm/s, CS = 0.45 (±0.01) mm/s, and 80% abundance and doublet 2 with QS = 1.96 (±0.15) mm/s,

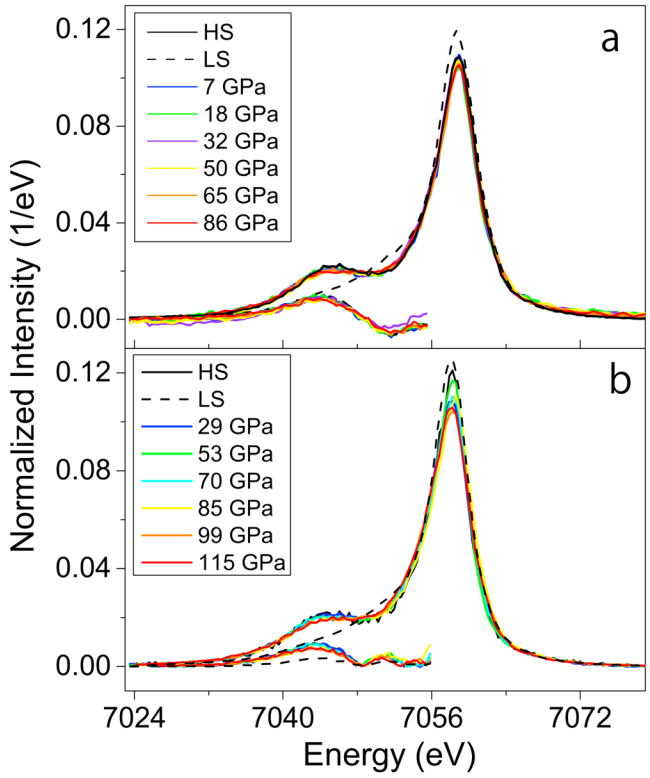

Figure 3. X-ray emission spectra of Fe Kβ of bridgmanite ($Mg_{0.89}Fe_{0.12}Al_{0.11}Si_{0.89}O_3$) at high pressures and ambient temperature (a) without laser annealing and (b) after laser annealing at ~1800 K at each given pressure. High-spin and low-spin references of ferropericlase ($(Mg_{0.75}Fe_{0.25})O$) at ambient conditions (solid black line) and at 95 GPa (dashed black line), respectively, are used for the data analysis. The differentials between the sample spectra and reference spectra are shown below the Fe Kβ′ spectral region up to 7056 eV for the integrated relative difference (IRD) analysis.

CS = 1.14 (±0.07) mm/s, and 20% abundance (Figure S1). Comparing these values with previous MS results and other relevant silicates indicates that the doublet 1 with 80% abundance can be assigned to high-spin Fe^{3+} in the A site and doublet 2 with 20% abundance to be high-spin Fe^{2+} in the A site (Figures S2 and S3) [e.g., *McCammon*, 1997; *Dyar et al.*, 2006; *Lin et al.*, 2012, 2013]. Based on the electron microprobe analyses of the crystals that showed an averaged chemical formula of $Mg_{0.89}Fe_{0.12}Al_{0.11}Si_{0.89}O_3$ with almost equal amounts of Fe^{3+} and Al^{3+} as well as 11% Si^{4+} deficiency and Al^{3+} substitution, we suggest, after considering the Mössbauer and electron microprobe results as well as the error of these measurements, that Al^{3+} substitutes for Si^{4+} in the B site via the charge-coupled substitution with Fe^{3+} in the A site, yielding a charge balance in the lattice [e.g., *Vanpeteghem et al.*, 2006; *Hummer and Fei*, 2012]. The SMS spectrum at 115 GPa after laser annealing was fitted with a three-doublet model: doublet 1 with QS 0.84 (±0.04) mm/s and 80% abundance, doublet 2 with QS = 1.81 (±0.15) mm/s and 14% abundance, and doublet 3 with QS = 3.21 (±0.25) mm/s and 6% abundance (Figure 2). Comparison of the analyzed Mössbauer results with literature values shows that the doublet 1 with 80% abundance and relatively low QS and CS can be assigned to the A-site Fe^{3+}, while doublet 2 and 3 with relatively high QS and CS values can be assigned to the A-site Fe^{2+} (Figures S2 and S3) [e.g., *McCammon*, 1997; *Ballaran et al.*, 2012; *Lin et al.*, 2012, 2013]. The relatively high abundance of the doublet 2 (14%) with a relatively low QS as compared with doublet 3 with lower abundance and higher QS in (Fe,Al)-bearing bridgmanite has been theoretically explained by the fact that the low-QS high-spin Fe^{2+} in the A site prefers a high volume and that (Fe^{3+},Al)-bearing bridgmanite has a larger volume than the Fe^{2+}-bearing counterpart [*Hsu et al.*, 2010, 2011, 2012]. Therefore, the results here indicate that the ratio of Fe^{3+} and Fe^{2+} in the A site remains unchanged at lower mantle pressure range after laser heating, supporting the dominant site occupancy in the A site and also negating the possibility of the proposed charge transfer in bridgmanite in the lower mantle.

High-pressure XES spectra collected from laser-annealed and nonannealed samples were analyzed using integrated absolute difference (IAD) and integrated relative difference (IRD) methods, respectively (Figures 3 and 4) [*Vanko et al.*, 2006; *Mao et al.*, 2014]. In the IAD analysis, the intensity of the Kβ satellite peak is integrated using reference high-spin and low-spin spectra in order to derive the integrated intensity of the iron ions in bridgmanite to infer its spin states at high pressures (Figure 3). These results show that the integrated intensity continuously decreases with increasing pressure by a maximum of 40% at the highest pressures for both annealed and nonannealed samples. However, it has been pointed out in the XES spectral analyses that broadening due to nonhydrostatic pressure can also lead to a decrease in the integrated intensity, leading to imprecise interpretation of the XES spectra [*Mao et al.*, 2014].

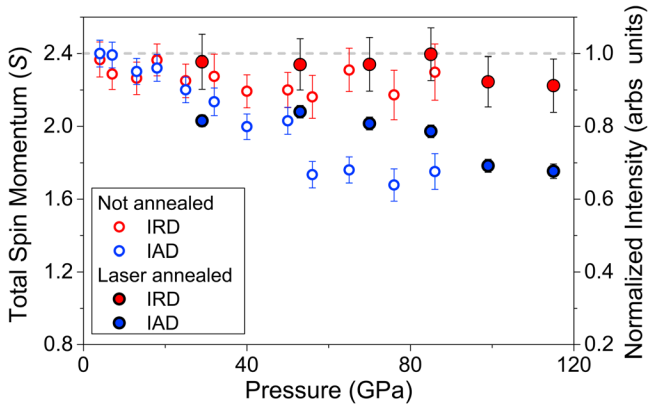

Figure 4. Total spin momentum of the Fe in the single-crystal aluminous bridgmanite ($Mg_{0.89}Fe_{0.12}Al_{0.11}Si_{0.89}O_3$) at high pressures and ambient temperature. The integrated intensity is normalized to one and zero using high-spin and low-spin ferropericlase, respectively, and is then used to infer the total spin momentum (*S*) using 80% Fe^{3+} and 20% Fe^{2+} in the lattice. Solid circles: data collected from the bridgmanite crystal after annealing at ~1800 K; open circles: data without annealing; red symbols: IRD method; blue symbols: IAD method. Horizontal dashed line is plotted to guide the eyes for the total spin momentum at 2.4.

The integrated intensity of the XES spectra from the IRD method, on the other hand, is systematically higher than that in the IAD method for both annealed and nonannealed samples (Figure 4). The IRD method has been shown to account for the pressure-induced peak broadening to allow for the integrated intensity to be more representative of the total spin momentum of iron in the sample [*Mao et al.*, 2014]. In the IRD analyses, the XES spectra are aligned around the Kβ main peak of the high-spin reference spectrum and are then integrated using the relative intensity difference of the spectra. Since the pressure-induced broadening effect on the XES spectra can produce spectral regions with either positive or negative differences in the comparison, the IRD analysis only integrates the difference in the satellite Kβ′ peak region from the lowest energy to the energy at approximately 7056 eV, where the spectral difference is zero near the left shoulder of the Kβ main peak. That is, the peak broadening effect from the Kβ main peak is minimized in the analysis. The difference in the integrated intensity between these two methods can be as large as approximately 30%, which can significantly affect the interpretation of the spin state of iron in the bridgmanite (Figure 4). In comparison, the integrated intensity for the annealed sample is systematically higher than that in the nonannealed samples in both IAD and IRD analyses (Figure 4). We interpret this difference as a result of the peak broadening under nonhydrostatic conditions in the nonannealed sample because laser annealing is expected to significantly reduce the nonhydrostatic stress and pressure gradient in the sample chamber. Considering the nonhydrostaticity in these experiments and the peak-broadening effect in the spectral analysis, the total spin momentum derived from the IRD analysis of the XES spectra collected from the annealed sample should provide the most reliable inference for the spin state of iron in bridgmanite at high pressures. Based on the Mössbauer analysis that shows 80% Fe^{3+} and 20% Fe^{2+} in the A site (Figure 2), the total spin momentum (*S*) of the iron ions should be 2.4 for the high-spin state and 0.4 for all iron in the low-spin state (Figure 4). Within the experimental uncertainties, our XES results show that the derived total spin momentum remains almost unchanged and is characteristic of high-spin iron in the A site of bridgmanite at pressures up to 115 GPa. Our complementary XES and SMS results also show that the A-site high-spin Fe^{3+} and Fe^{2+} mostly remain in the same crystallographic site even after laser annealing at high pressures, indicating that the B-site Fe^{3+} which will undergo a spin transition at high pressures is very minor in lower mantle (Fe,Al)-bearing bridgmanite. These results are consistent with recent theoretical predictions [*Hsu et al.*, 2012; *Mohna and Trønnesa*, 2016] but are at odds with some experimental reports that suggested the charge transfer between the A-site Fe^{2+} and the B-site Fe^{3+} occurs at lower mantle conditions [e.g., *Fujino et al.*, 2012, 2014].

4. Geophysical Implications

Our high-pressure results here reconcile recent experimental and theoretical results to show that (Fe,Al)-bearing bridgmanite in the lower mantle predominantly contains stable high-spin Fe^{2+} and Fe^{3+} in the distorted A site, in which most iron ions are Fe^{3+}. In a pyrolite compositional model, Earth's lower mantle is expected to contain ~7 wt % Al_2O_3 that dissolves into bridgmanite from majoritic garnet with increasing pressure from 23 GPa to ~28 GPa (660 km to ~770 km in depth) [e.g., *Irifune et al.*, 2010]. The dissolution of Al^{3+} in turn would enrich the bridgmanite lattice with Fe^{3+} in the A site; such that, only a small amount of the B-site Fe^{3+} is expected to exist below the top lower mantle conditions [e.g., *Hummer and Fei*, 2012; *Potapkin et al.*, 2013;

Mohna and Trønnesa, 2016; *Muir and Brodholt*, 2016]. Therefore, even though the B-site Fe^{3+} in bridgmanite has been reported to transition to the low-spin state at high pressures [e.g., *Catalli et al.*, 2011; *Hsu et al.*, 2012; *Lin et al.*, 2012; *Mao et al.*, 2015; *Muir and Brodholt*, 2016], the negligible amount of the B-site Fe^{3+} in (Fe,Al)-bearing bridgmanite is unlikely to play a major role in influencing the lower mantle geophysics and geochemistry. These results also indicate that the dominant A-site Fe^{3+} does not migrate to the B site at relevant lower mantle conditions.

Considering that bridgmanite and ferropericlase are the most abundant minerals in the lower mantle, one can now address the collective role of the site occupancy and spin and valence states of iron on the lower mantle geochemistry and seismology. Recent high *P-T* studies have shown that the partition coefficient of iron between bridgmanite (Bm) and ferropericlase (Fp), ($K_D^{Bm\text{-}Fp} = (Fe/Mg)_{Bm}/(Fe/Mg)_{Fp}$), can be drastically influenced by the Al^{3+} substitution in bridgmanite and the spin transition of iron in ferropericlase, leading to high-spin bridgmanite enriched in Fe^{3+} at the top lower mantle while the low-spin, iron-enriched ferropericlase coexists with iron-depleted bridgmanite below the middle-lower mantle conditions [e.g., *Irifune et al.*, 2010; *Muir and Brodholt*, 2016]. Together with the stable high-spin bridgmanite throughout the lower mantle observed here, the spin transition of iron in ferropericlase is thus expected to play a dominant progressive role on the geophysics and geochemistry below the middle-lower mantle [e.g., *Yang et al.*, 2015]. These results are mostly consistent with recent seismic observations of the lower mantle, where the top to middle parts of the lower mantle are mostly seismically homogeneous [e.g., *Grand et al.*, 1997; *Gu et al.*, 2001; *Lekic et al.*, 2012; *van der Hilst and Karason*, 1999]. The conventional seismic observations for a relatively homogeneous region above the middle parts of the lower mantle are thus safe. However, our study here calls for further reexamination of some previous studies that have reported significant influences of the spin transitions of iron on physical, chemical, and transport properties of bridgmanite in the lower mantle [e.g., *Goncharov et al.*, 2008; *Keppler et al.*, 2008; *Ohta et al.*, 2010].

Acknowledgments

We acknowledge N. Purevjav, N. Tomiaka, V. Prapapenka, Y. Hong, J. Zhao, and B. Li for their assistance. We also thank H. Hsu and S. Jacobsen for their constructive comments. J.F. Lin acknowledges supports from the Geophysics and CSEDI Programs of the NSF and the Visiting Professorship Program of the Okayama University. We also thank C. McCammon for analyzing the Mössbauer spectrum of the crystals at ambient conditions. Portions of this work were performed at HPCAT, GSECARS, and XOR3 sectors of the APS. HPCAT is supported by CIW, CDAC, UNLV, and LLNL through funding from DOE-NNSA, DOE-BES, and NSF. APS is supported by 263 DOE-BES, under contract DE-AC02-06CH11357. Part of this work by T.O. was supported by JSPS KAKENHI (26287135). Experimental data have been shown in Figures 1–4, S1, and S2.

References

Badro, J., G. Fiquet, F. Guyot, J. P. Rueff, V. V. Struzhkin, G. Vankó, and G. Monaco (2003), Iron partitioning in Earth's mantle: Toward a deep lower mantle discontinuity, *Science*, *300*, 789–791.

Badro, J., J. P. Rueff, G. Vankó, G. Monaco, G. Fiquet, and F. Guyot (2004), Electronic transitions in perovskite: Possible nonconvecting layers in the lower mantle, *Science*, *305*, 383–386.

Ballaran, T. B., A. Kurnosov, K. Glazyrin, D. J. Frost, M. Merlini, M. Hanfland, and R. Caracas (2012), Effect of chemistry on the compressibility of silicate perovskite in the lower mantle, *Earth Planet. Sci. Lett.*, *333–334*, 181–190.

Bengtson, A., K. Persson, and D. Morgan (2008), Ab initio study of the composition dependence of the pressure induced spin crossover in perovskite ($Mg_{1-x}Fe_x)SiO_3$, *Earth Planet. Sci. Lett.*, *265*, 535–545.

Bengtson, A., J. Li, and D. Morgan (2009), Mössbauer modeling to interpret the spin state of iron in $(Mg,Fe)SiO_3$ perovskite, *Geophys. Res. Lett.*, *36*, L15301, doi:10.1029/2009GL038340.

Cammarano, F., H. Marquardt, S. Speziale, and P. J. Tackley (2010), Role of iron-spin transition in ferropericlase on seismic interpretation: A broad thermochemical transition in the mid mantle?, *Geophys. Res. Lett.*, *37*, L03308, doi:10.1029/2009GL041583.

Catalli, K., S. H. Shim, V. B. Prakapenka, J. Zhao, W. Sturhahn, P. Chow, Y. Xiao, H. Liu, H. Cynn, and W. J. Evans (2010), Spin state of ferric iron in $MgSiO_3$ perovskite and its effect on elastic properties, *Earth Planet. Sci. Lett.*, *289*, 68–75.

Catalli, K., S.-H. Shim, P. Dera, V. B. Prakapenka, J. Zhao, W. Sturhahn, P. Chow, Y. Xiao, H. Cynn, and W. J. Evans (2011), Effects of the Fe^{3+} spin transition on the properties of aluminous perovskite—New insights for lower-mantle seismic heterogeneities, *Earth Planet. Sci. Lett.*, *310*, 293–302.

Dyar, M. D., D. G. Agresti, M. W. Schaefer, C. A. Grant, and E. C. Sklute (2006), Mössbauer spectroscopy of Earth and planetary materials, *Annu. Rev. Earth Planet. Sci.*, *34*, 83–125.

Fei, Y. W., A. Ricolleau, M. Frank, K. Mibe, G. Y. Shen, and V. Prakapenka (2007), Toward an internally consistent pressure scale, *Proc. Natl. Acad. Sci. U.S.A.*, *104*(22), 9182–9186.

Fujino, K., et al. (2012), Spin transition of ferric iron in Al-bearing Mg-perovskite up to 200 GPa and its implication for the lower mantle, *Earth Planet. Sci. Lett.*, *317–318*, 407–412.

Fujino, K., D. Nishio-Hamane, T. Nagai, Y. Seto, Y. Kuwayama, M. Whitaker, H. Ohfuji, T. Shinmei, and T. Irifune (2014), Spin transition, substitution, and partitioning of iron in lower mantle minerals, *Phys. Earth Planet. Inter.*, *228*, 186–191.

Goncharov, A. F., B. D. Haugen, V. V. Struzhkin, P. Beck, and S. D. Jacobsen (2008), Radiative thermal conductivity in the Earth's lower mantle, *Nature*, *456*, 231–234.

Grand, S. P., R. D. van der Hilst, and S. Widiyantoro (1997), Global seismic tomography: A snapshot of convection in the Earth, *GSA Today*, *7*, 1–7.

Grocholski, B., S. H. Shim, W. Sturhahn, J. Zhao, Y. Xiao, and C. Chow (2009), Spin and valence states of iron in $(Mg_{0.8}Fe_{0.2})$ SiO_3 perovskite, *Geophys. Res. Lett.*, *36*, L24303, doi:10.1029/2009GL041262.

Gu, Y., A. Dziewonski, W. Su, and G. Ekstrom (2001), Models of the mantle shear velocity and discontinuities in the pattern of lateral heterogeneities, *J. Geophys. Res.*, *106*(B6), 11,169–11,199, doi:10.1029/2001JB000340.

Hsu, H., and R. M. Wentzcovitch (2014), First-principles study of intermediate-spin ferrous iron in the Earth's lower mantle, *Phys. Rev. B*, *90*, 195205.

Hsu, H., K. Umemoto, P. Blaha, and R. M. Wentzcovitch (2010), Spin states and hyperfine interactions of iron in $(Mg,Fe)SiO_3$ perovskite under pressure, *Earth Planet. Sci. Lett.*, *294*, 19–26.

Hsu, H., P. Blaha, M. Cococcioni, and R. M. Wentzcovitch (2011), Spin-state crossover and hyperfine interactions of ferric iron in $MgSiO_3$ perovskite, *Phys. Res. Lett.*, *106*, 118501.

Hsu, H., Y. G. Yu, and R. M. Wentzcovitch (2012), Spin crossover of iron in aluminous $MgSiO_3$ perovskite and post-perovskite, *Earth Planet. Sci. Lett.*, *294*, 19–26.

Hummer, D., and Y. Fei (2012), Synthesis and crystal chemistry of Fe^{3+}-bearing $(Mg,Fe^{3+})(Si,Fe^{3+})O_3$ perovskite, *Am. Mineral.*, *97*, 1915–1921.

Irifune, T., T. Shinmei, C. A. McCammon, N. Miyajima, D. C. Rubie, and D. J. Frost (2010), Iron partitioning and density changes of pyrolite in Earth's lower mantle, *Science*, *327*, 193–195.

Jackson, J. M., W. Sturhahn, G. Shen, J. Zhao, M. Y. Hu, D. Errandonea, J. D. Bass, and Y. Fei (2005), A synchrotron Mössbauer spectroscopy study of $(Mg,Fe)SiO_3$ perovskite up to 120 GPa, *Am. Mineral.*, *90*, 199–205.

Keppler, H., L. S. Dubrovinski, O. Narygina, and I. Kantor (2008), Optical absorption and radiative thermal conductivity of silicate perovskite to 125 GPa, *Science*, *322*, 1529–1532.

Lekic, V., S. Cottaar, A. M. Dziewonski, and B. Romanowicz (2012), Cluster analysis of global lower mantle tomography: A new class of structure and implications for chemical heterogeneity, *Earth Planet. Sci. Lett.*, *357–358*, 68–77.

Li, J., V. V. Struzhkin, H. K. Mao, J. Shu, R. J. Hemley, Y. Fei, B. Mysen, P. Dera, V. Prakapenka, and G. Shen (2004), Electronic spin state of iron in lower mantle perovskite, *Proc. Natl. Acad. Sci. U.S.A.*, *101*, 14,027–14,030.

Li, J., W. Sturhahn, J. M. Jackson, V. V. Struzhkin, J. F. Lin, J. Zhao, H. K. Mao, and G. Shen (2006), Pressure effect on the electronic structure of iron in $(Mg,Fe)(Si,Al)O_3$ perovskite: A combined synchrotron Mössbauer and X-ray emission spectroscopy study up to 100 GPa, *Phys. Chem. Miner.*, *33*, 575–585.

Lin, J. F., V. V. Struzhkin, S. D. Jacobsen, M. Hu, P. Chow, J. Kung, H. Liu, H. K. Mao, and R. J. Hemley (2005), Spin transition of iron in magnesiowüstite in Earth's lower mantle, *Nature*, *436*, 377–380.

Lin, J. F., et al. (2008), Intermediate-spin ferrous iron in lowermost mantle post-perovskite and perovskite, *Nat. Geosci.*, *1*, 688–691.

Lin, J. F., E. E. Alp, Z. Mao, T. Inoue, C. McCammon, Y. Xiao, P. Chow, and J. Zhao (2012), Electronic spin and valence states of iron in the lower-mantle silicate perovskite by synchrotron Mössbauer spectroscopy, *Am. Mineral.*, *97*, 592–597.

Lin, J. F., S. Speziale, Z. Mao, and H. Marquardt (2013), Effects of the electronic spin transitions of iron in lower-mantle minerals: Implications to deep-mantle geophysics and geochemistry, *Rev. Geophys.*, *51*, 244–275, doi:10.1002/rog.20010.

Mao, H. K., J. Xu, and P. M. Bell (1986), Calibration of the ruby pressure gauge to 800 kbar under quasi-hydrostatic conditions, *J. Geophys. Res.*, *91*, 4673–4676, doi:10.1029/JB091iB05p04673.

Mao, Z., J. F. Lin, H. P. Scott, H. Watson, V. B. Prakapenka, Y. Xiao, and P. Chow (2011), Stiff iron-rich silicate perovskite in the large low shear velocity provinces, *Earth Planet. Sci. Lett.*, *309*, 179–184.

Mao, Z., J. F. Lin, J. Yang, J. Wu, H. C. Watson, Y. Xiao, P. Chow, and J. Zhao (2014), Spin and valence state of iron in Al-bearing silicate glass at high pressures studied by synchrotron Mössbauer and X-ray emission spectroscopy, *Am. Mineral.*, *99*, 415–423.

Mao, Z., J. F. Lin, J. Yang, T. Inoue, and V. B. Prakapenka (2015), Effects of the Fe^{3+} spin transition on the equation of state of bridgmanite, *Geophys. Res. Lett.*, *42*, 4335–4342, doi:10.1002/2015GL064400.

McCammon, C. (1997), Perovskite as a possible sink for ferric iron in the lower mantle, *Nature*, *387*, 694–696.

McCammon, C. (2006), Microscopic properties to macroscopic behavior: The influence of iron electronic states, *J. Mineral. Petrol. Sci.*, *101*, 130–144.

McCammon, C., I. Kantor, O. Narygina, J. Rouquette, U. Ponkratz, I. Sergueev, M. Mezouar, V. B. Prakapenka, and L. Dubrovinsky (2008), Stable intermediate-spin ferrous iron in lower mantle perovskite, *Nat. Geosci.*, *1*, 684–687.

McCammon, C., L. Dubrovinsky, O. Narygina, I. Kantor, X. Wu, K. Glazyrin, I. Sergueev, and A. I. Chumakov (2010), Low-spin Fe^{2+} in silicate perovskite and a possible layer at the base of the lower mantle, *Phys. Earth Planet. Inter.*, *180*, 215–221.

Mohna, C. E., and R. G. Trønnesa (2016), Iron spin state and site distribution in $FeAlO_3$-bearing bridgmanite, *Earth Planet. Sci. Lett.*, *440*, 178–186.

Muir, J. M. R., and J. P. Brodholt (2016), Ferrous iron partitioning in the lower mantle, *Phys. Earth Planet. Inter.*, doi:10.1016/j.pepi.2016.05.008.

Ohta, K., K. Hirose, K. Shimizu, N. Sata, and Y. Ohishi (2010), The electrical resistance measurements of $(Mg,Fe)SiO_3$ perovskite at high pressures and implications for electronic spin transition of iron, *Phys. Earth Planet. Inter.*, *180*, 154–158.

Okuchi, T., N. Purevjav, N. Tomioka, J. F. Lin, T. Kuribayashi, L. Schoneveld, H. Hwang, N. Sakamoto, N. Kawasaki, and H. Yurimoto (2015), Synthesis of large and homogeneous single crystals of deep-mantle hydrous minerals by slow cooling quenching at transition zone to lower deep-mantle pressures, *Am. Mineral.*, *100*, 1483–1492.

Potapkin, V., et al. (2013), Effect of iron oxidation state on the electrical conductivity of the Earth's lower mantle, *Nat. Commun.*, *4*, doi:10.1038/Ncomms2436.

Speziale, S., A. Milner, V. E. Lee, S. M. Clark, M. P. Pasternak, and R. Jeanloz (2005), Iron spin transition in Earth's mantle, *Proc. Natl. Acad. Sci. U.S.A.*, *102*, 17,918–17,922.

Sturhahn, W. (2000), CONUSS and PHOENIX: Evaluation of nuclear resonant scattering data, *Hyperfine Interact.*, *125*, 149–172.

van der Hilst, R. D., and H. Karason (1999), Compositional heterogeneity in the bottom 1000 kiometers of Earth's mantle: Toward a hybrid convection model, *Science*, *283*, 578–584.

Vanko, G., T. Neisius, G. Molnar, F. Renz, S. Karpati, A. Shukla, and F. M. F. de Groot (2006), Probing the 3D spin momentum with X-ray emission spectroscopy: The case of molecular-spin transitions, *J. Phys. Chem. B*, *110*, 11,647–11,653.

Vanpeteghem, C. B., R. J. Angel, N. L. Ross, S. D. Jacobsen, D. P. Dobson, K. D. Litasov, and E. Ohtani (2006), Al, Fe substitution in the $MgSiO_3$ perovskite structure: A single-crystal X-ray diffraction study, *Phys. Earth Planet. Inter.*, *155*(1–2), 96–103.

Yang, Y., X. Tong, J. F. Lin, N. Tomioka, T. Okuchi, and V. B. Prakapenka (2015), Elasticity of ferropericlase across the spin crossover in the Earth's lower mantle, *Sci. Rep.*, *5*, 17188.